Journal of the Mechanics and Physics of Solids 61 (2013) 293–310

Contents lists available at SciVerse ScienceDirect

Journal of the Mechanics and Physics of Solids

journal homepage: www.elsevier.com/locate/jmps

Interface-reaction controlled diffusion in binary solids with applications to lithiation of silicon in lithium-ion batteries

Zhiwei Cui [a], Feng Gao [a], Jianmin Qu [a,b,*]

[a] Department of Civil and Environmental Engineering, Northwestern University, Evanston, IL 60208, USA
[b] Department of Mechanical Engineering, Northwestern University, Evanston, IL 60208, USA

ARTICLE INFO

Article history:
Received 4 July 2012
Received in revised form
27 September 2012
Accepted 7 November 2012
Available online 16 November 2012

Keywords:
Lithium-ion battery
Interface
Diffusion
Chemical reaction
Amorphization

ABSTRACT

Solid state diffusion in a binary system, such as lithiation into crystalline silicon, often involves two symbiotic processes, namely, interfacial chemical reaction and bulk diffusion. Building upon our earlier work (Cui et al., 2012b, J. Mech. Phys. Solids, 60 (7), 1280–1295), we develop a mathematical framework in this study to investigate the interaction between bulk diffusion and interfacial chemical reaction in binary systems. The new model accounts for finite deformation kinematics and stress–diffusion interaction. It is applicable to arbitrary shape of the phase interface. As an example, the model is used to study the lithiation of a spherical silicon particle. It is found that a dimensionless parameter $\beta = k_f^e V_m^B R_0/D_0$ plays a significant role in determining the kinetics of the lithiation process. This parameter, analogous to the Biot number in heat transfer, represents the ratio of the rate of interfacial chemical reaction and the rate of bulk diffusion. Smaller β means slower interfacial reaction, which would result in higher and more uniform concentration of lithium in the lithiated region. Furthermore, for a given β, the lithiation process is always controlled by the interfacial chemical reaction initially, until sufficient silicon has been lithiated so that the diffusion distance for lithium reaches a threshold value, beyond which bulk diffusion becomes the slower process and controls the overall lithiation kinetics.

1. Introduction

Solid-state diffusion often involves chemical reaction. The subject has been studied extensively with applications to, for example, powder-based sintering (Deb and Pitchumani 2011; Yalamac et al., 2011), oxidation growth (Hou et al., 2012), diffusion bonding (Qian et al., 2011), redox in ionic systems (Tikekar et al., 2006), etc. In this class of problems, the diffusion species first reacts chemically with the host solvent to form a third phase, and the reaction occurs mainly on the interface between the solvent and this third phase. The reaction is sustained by the diffusion species through the newly formed third phase material. As a result, a sharp interface is often developed between the phases. Since the chemical reaction takes place at the interface, the kinetics of the surface chemical reaction dictates the interface motion. Generally speaking, there are three regimes. First, the interface chemical reaction rate is much faster than the rate of bulk diffusion, which means that the velocity of the interface can be assumed infinitely large, thus one only needs to solve the diffusion

* Corresponding author at: Northwestern University, Department of Civil and Environmental Engineering, Department of Mechanical Engineering, Evanston, IL 60208, USA. Tel.: +1 847 467 4528.
E-mail address: j-qu@northwestern.edu (J. Qu).

0022-5096/$ - see front matter © 2012 Elsevier Ltd. All rights reserved.
http://dx.doi.org/10.1016/j.jmps.2012.11.001

equation. In this case, the process is fully controlled by the bulk diffusion. Second, the interfacial chemical reaction rate is much slower than the rate of bulk diffusion, which means that the process is fully controlled by the surface chemical reaction. In this case, the newly formed third phase is fully saturated with the diffusion species, and the interface motion can be determined by the interfacial chemical reaction rate through mass conservation. The third regime is the case when the interfacial chemical reaction rate is comparable to the rate of bulk diffusion. In this case, both the interface velocity and the diffusion equation must be solved together.

Various models have been developed to describe such chemical reaction controlled solid state diffusions, e.g., (Murray and Carey 1988a,b, 1989a,b, 1990; Filipek, 2005; Furuto and Kajihara, 2008; Gotze et al., 2010; Abart and Petrishcheva, 2011; Abart et al., 2012). A good summary of the different models can be found in the monograph (Dybkov, 2010). There is also a class of problems in heat transfer that are analogous to such reaction controlled diffusion such as melting of ice and solidification (Reemtsen and Kirsch, 1984; Caldwell and Kwan, 2004; Ramos, 2005; Ang, 2008; Caldwell and Kwan, 2009).

Recently, silicon (Si) has attracted significant attention because of its potential as a high capacity anode material in lithium (Li) ion batteries. Extensive effort has been invested in the last decade to understand the lithiation process. Earlier studies in this area modeled lithiation as a diffusion-controlled process, from which Li distribution can be computed (Bower et al., 2011; Cui et al., 2012b). However, recent experimental observation show that there is a sharp interface between lithiated and unlithiated phases, indicating that the lithiation process may be controlled by interfacial chemical reaction (Chan et al., 2008; Cui et al., 2009; Chon et al., 2011; Lee et al., 2011; Liu and Huang, 2011; Lee et al., 2012; Liu et al., 2012; Yang et al., 2012).

Although there exists a comprehensive literature on modeling of reaction-controlled solid state diffusion as referenced above, material systems such as Li_xSi have certain unique properties that the existing theories of reaction-controlled diffusion are not applicable. First, lithiation into Si generates a very large volumetric change ($\sim$400%) (Cui et al., 2009; Liu and Huang, 2011). Because of such large volumetric change, finite kinematics must be used to describe the deformation during lithiation. Existing theories are all based on small strain deformation. Second, such large volumetric change, if not accommodated by appropriate deformation, will generate mechanical stresses, which will in turn affect the diffusion (Swaminathan and Qu, 2007; Swaminathan et al., 2007a,b; Swaminathan and Qu, 2009; Cui et al., 2012b). None of the existing theories accounts for such two-way interaction. Third, most existing theories implicitly assume first order chemical reaction at the interface between the phases. This severely limits their applicability to cases with more complex interfacial chemical reactions.

In this paper, we will develop a rigorous mathematical framework to describe the interface-reaction controlled diffusion in binary solids such as Li_xSi. This framework is developed based on finite deformation kinematics. It is capable of accounting for diffusion–stress interaction, and applicable to interfacial chemical reaction of arbitrary order. As an example, the lithiation of a spherical Si particle is solved to illustrate the application of the general model developed.

We need to point out that a number of recent studies have focused on modeling the lithiation of Si particles and wires in an effort to model the sharp interface observed in the experiments. For example, Zhang and White (2007) proposed a numerical model to describe the moving boundary for the discharge of a $LiCoO_2$ electrode, in which a sharp interface with abrupt concentration drop was modeled. A similar approach was adopted to model the diffusion induced stress and strain energy in a Si spherical electrode particle (Deshpande et al., 2011). In all these models, the interfacial chemical reactions are not considered. Instead, the sharp interface is generated by using different bulk diffusivities between the Si and Li_xSi phases. Zhao et al. (2012) did consider interfacial chemical reaction. However, the interface velocity in their model is assumed given a priori that is independent of the kinetics of chemical reaction at the interface.

2. Problem statement

Consider a solid phase called the α-phase consisting of species A, and another solid phase called the β-phase consisting of species B. Let the two phases be in intimate contact initially, see Fig. 1a. Assume that under certain driving forces (e.g., chemical affinity or externally applied voltage), species A starts to react with species B to form a new phase called the γ-phase, which consists of species $P=A_{x_0}B$, i.e.,

$$x_0 A + B \rightarrow A_{x_0} B \tag{1}$$

As time progresses, species A diffuses through the γ-phase towards the β-phase, and reacts continuously with species B at the β–γ interface. This sustained reaction produces more species P and drives the interface move further into the β-phase, see Fig. 1b. For simplicity, we assume that the β-phase is impervious to species A, and, as the interface moves, species B is fully converted into the γ-phase at the β–γ interface via the interfacial chemical reaction (1). Our main interest is to find the shape and velocity of the β–γ interface, and the concentration of species A in the γ-phase.

As will be seen later, this problem involves deformation, diffusion and chemical reaction. In what follows, we will derive the governing equations for these processes and the corresponding boundary and initial conditions.

3. Deformation and mechanical equilibrium

For convenience, we will employ two ways to describe the deformation and motion of the solids, namely, the Lagrangian (or the referential) description and the Eulerian (or the spatial) description. We will use **X** and **x** to represent

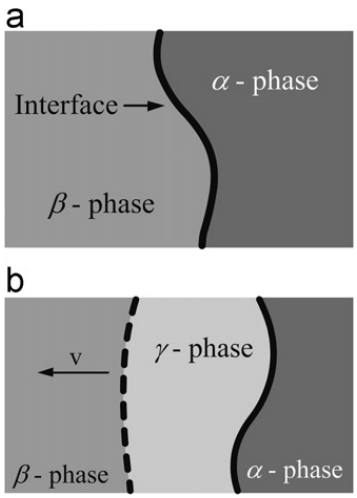

Fig. 1. Schematic of the (a) initial configuration and (b) current configuration.

the coordinates in the Lagrangian and Eulerian descriptions, respectively. In other words, **X** is the label of a material point located at location **X** initially ($t=0$). At a current time t, this particle **X** is located at **x**. This relationship can be symbolically written as $\mathbf{x}=\mathbf{x}(\mathbf{X},t)$. Inversely, one can think of a fixed spatial location **x**. At a given time t, there will be a material particle called **X** happens to be located at this fixed location. At a different time, a different particle will be found at **x**, i.e., at different times, the material particle located at **x** is different. Therefore, the material particle found at location **x** at time t can be symbolically identified as $\mathbf{X}=\mathbf{X}(\mathbf{x},t)$. In what follows, we assume that all field quantities are written as functions of **X**, unless stated explicitly otherwise.

Based on the above definition, one can easily define the displacement of a particle

$$\mathbf{U}(\mathbf{X},t)=\mathbf{x}-\mathbf{X}, \tag{2}$$

in the Lagrangian description. This naturally leads to its corresponding deformation gradient tensor

$$\mathbf{F}=\nabla_X\mathbf{x}=\mathbf{I}+\nabla_X\mathbf{U}(\mathbf{X},t), \tag{3}$$

where ∇_X is the gradient operator with respect to the coordinates **X**

In this paper, we will used $\mathbf{F}_\beta$ and $\mathbf{F}_\gamma$ to denote the deformation gradient tensors in the β-phase and the γ-phase, respectively. We further assume that, for simplicity, the β-phase undergoes only elastic deformation. In the γ-phase, however, inelastic deformation may develop due to the compositional change. Following from Cui et al. (2012b), we write

$$\mathbf{F}_\gamma=\mathbf{F}^e\mathbf{F}^*,\ \ \mathbf{F}^*=\mathbf{F}^c\mathbf{F}^p, \tag{4}$$

where $\mathbf{F}^c$ represents the eigen-transformation due to the compositional change, $\mathbf{F}^p$ represents the plastic deformation, and $\mathbf{F}^e$ represents the elastic deformation associated with $\mathbf{F}^*$so that the total deformation is compatible.

Eq. (4) represents a deformation that transforms the initial (undeformed) state of the solid to its final (current or deformed) state. The total deformation can be viewed as a sequence of eigen-transformation represented by $\mathbf{F}^*$ followed by an elastic deformation represented by $\mathbf{F}^e$. The state of the solid after the eigen-transformation $\mathbf{F}^*$ is called the intermediate state. We note that the intermediate state is a stress-free state, and is not necessarily kinematically compatible.

It follows from the first of (4) that the total Lagrange strain can be written as

$$\mathbf{E}=\frac{1}{2}\left(\mathbf{F}^T\mathbf{F}-\mathbf{I}\right)=\left(\mathbf{F}^c\mathbf{F}^p\right)^T\mathbf{E}^e\mathbf{F}^c\mathbf{F}^p+\left(\mathbf{F}^p\right)^T\mathbf{E}^c\mathbf{F}^p+\mathbf{E}^p, \tag{5}$$

where

$$\mathbf{E}^e=\frac{1}{2}\left[\left(\mathbf{F}^e\right)^T\mathbf{F}^e-\mathbf{I}\right],\ \mathbf{E}^c=\frac{1}{2}\left[\left(\mathbf{F}^c\right)^T\mathbf{F}^c-\mathbf{I}\right],\ \mathbf{E}^p=\frac{1}{2}\left[\left(\mathbf{F}^p\right)^T\mathbf{F}^p-\mathbf{I}\right], \tag{6}$$

can be regarded, at least symbolically, as the elastic strain, compositional strain, and the plastic strain, respectively. At this point, it is necessary to introduce the constitutive equations that relate the different strain measures to either the stress or the composition. For example, Hooke's law may be used to express stresses in terms of the elastic strains, and elastic-plastic law may be used to relate the stress to the plastic strain or plastic strain rate. As for the compositional strain, one may use (Cui et al., 2012b) $\mathbf{F}^c=\left(J^c\right)^{1/3}\mathbf{I}$, where $J^c=1+3\eta x_{\max}c$, $x_{\max}$ is the solubility of species A in the γ-phase, c is the molar fraction of species A in the γ-phase, and η is the coefficient of compositional expansion (CCE), which is a material property that characterizes the linear measure of the volumetric change due to unit change of the concentration (Swaminathan et al., 2007a,b). For a given material, the CCE can be obtained either experimentally, or by conducting molecular dynamic simulations (Swaminathan and Qu, 2009; Cui et al., 2011).

Use of these constitutive equations enable us to express the stress in terms of the three components of the displacement vector $\mathbf{U}(\mathbf{X},t)$. The state of stress at a point in a continuum can be represented by the first Piola–Kirchhoff (P–K) stress, which needs to satisfy the following equilibrium equation

$$\nabla_X \times \boldsymbol{\sigma}^0 = 0 \tag{7}$$

Based on the foregoing discussions, this equilibrium equation represents three scalar equations for the three components of the displacement vector $\mathbf{U}(\mathbf{X},t)$. Of course, it also contains the molar fraction c, which will be discussed in details in the next section.

The solution to (7) depends on the boundary conditions which will need to be prescribed

$$\mathbf{U}(\mathbf{X},t)\big|_{S_u} = \mathbf{U}_0(t), \qquad \boldsymbol{\sigma}^0 \times \mathbf{N}\big|_{S_\sigma} = \mathbf{P}_0(t), \tag{8}$$

where S_u and S_σ are portions of the boundary where displacement and tractions are given, respectively.

4. Diffusion

Let $x_{\max}$ be the solubility of species A in the γ-phase, i.e., the maximum number of moles of species A that each mole of species B is capable of containing. Based on the reaction described by (1), we may then introduce the molar fraction as $c=(x+x_0)/x_{\max}$ to describe the deviation from stoichiometry of species A in the γ-phase, which is also a measure of the concentration of species A in the nonstoichiometric state of the γ-phase, i.e., $A_{x_0+x}B$. Note that such a molar fraction is a dimensionless (or normalized) quantity, which is independent of any reference frames. Clearly, we have $0\le c\le 1$. If the reaction described by (1) is irreversible, i.e., the γ-phase cannot be dissolved or decomposed, we have $x_0/x_{\max}\le c\le 1$. For $0\le c\le x_0/x_{\max}$, one must have $-x_0\le x\le 0$, which means the depletion of species A from the γ-phase.

The molar concentration of species A in $A_{x+x_0}B$ in the Lagrangian description is given by

$$\rho_{\mathrm{A}} = \frac{x_{\max} c}{V_m^B} \quad in \ \gamma\text{-phase}, \tag{9}$$

where V_m^{B} is the initial molar volume of the β-phase (undeformed state). Similarly, the Lagrangian molar concentration of the product $\mathrm{P}=A_{x_0}B$ in the γ-phase, and the Lagrangian molar concentration of species B in the β-phase can be defined as, respectively,

$$\rho_{\mathrm{P}} = \frac{1}{V_m^B} \quad in \ \gamma\text{-phase}, \quad \text{and} \quad \rho_{\mathrm{B}} = \frac{1}{V_m^B} \quad in \ \beta\text{-phase} \tag{10}$$

To study the diffusion of species A in the γ-phase, we will adopt the stress-dependent chemical potential, or more precisely the diffusion potential of species A in the γ-phase (Cui et al., 2012b),

$$\mu(\mathbf{F},c) = \mu_0 + R_g T \log(\gamma c) + \tau(\mathbf{F},c), \tag{11}$$

$$\tau(\mathbf{F},c) = \frac{V_m^B}{x_{\max}}\left[\boldsymbol{\Sigma}\mathbf{f}^*\left(\frac{\partial \mathbf{F}^*}{\partial c}\right)_{\mathbf{F},\mathbf{C}} + J^*\left(\frac{\partial w(\mathbf{F},c)}{\partial c}\right)_{\mathbf{F}^e,\mathbf{F}^*}\right], \tag{12}$$

where μ_0 is a constant represents the chemical potential at a standard state, R_g is the standard gas constant, T is the absolute temperature in Kelvin, and γ is the activity coefficient, $\boldsymbol{\Sigma}$ is the Eshelby stress tensor, $w(\mathbf{F},c)$ is the strain energy per unit volume of the intermediate state, and $J^*=\det(\mathbf{F}^*)$, $\mathbf{f}^*=(\mathbf{F}^*)^{-1}$.

The molar flux of species A in the γ-phase per unit Lagrangian area is given by

$$\mathbf{J} = -\frac{D\rho_A}{R_g T}\mathbf{F}_\gamma^{-1}\left(\mathbf{F}_\gamma^{-1}\right)^T \nabla_{\mathbf{X}}\mu = -\frac{1}{R_g T}\frac{D x_{\max} c}{V_m^{\mathrm{B}}}\mathbf{F}_\gamma^{-1}\left(\mathbf{F}_\gamma^{-1}\right)^T \nabla_{\mathbf{X}}\mu, \tag{13}$$

where D is the diffusion coefficient of species A in the γ-phase in the current state, which may be dependent on the deformation gradient $\mathbf{F}$ and the molar fraction c. Now, consider an arbitrary Lagrangian volume V in the γ-phase. It then follows that the total number of moles of species A in V is given by

$$M = \int_V \rho_A dV, \tag{14}$$

The rate of increase (moles/time) in the volume V is thus given by

$$\frac{\partial M}{\partial t} = \int_V \frac{\partial \rho_A}{\partial t} dV = \int_V \frac{x_{\max}\partial c}{V_m^{\mathrm{B}}\partial t} dV, \tag{15}$$

where, in deriving the second equality, we have used (9).

On the other hand, the net inflow of species A into the volume V is given by

$$-\int_S \mathbf{J}\mathbf{N} dS = -\int_V \nabla_X \mathbf{J} dV, \tag{16}$$

where S is the surface enclosing V, $\mathbf{N}$ is the outward unit normal of S, and $\mathbf{J}$ is the flux of species A given in (13).

The equality in (16) is a result of the divergence theorem. Conservation of moles of species A inside the volume V then dictates that (15) and (16) must be equal, i.e.,

$$\int_V \frac{x_{\max}\partial c}{V_m^{\mathrm{B}}\partial t}dV = -\int_V \nabla_X \mathbf{J} dV \tag{17}$$

Since the volume V can be arbitrary, the localized version of (17) leads to the continuity equation in the γ-phase,

$$\frac{x_{\max}\partial c}{V_m^{\mathrm{B}}\partial t} + \nabla_X \mathbf{J} = 0 \tag{18}$$

To solve the above diffusion equation, initial and boundary values need to be prescribed. For the initial condition, one can simply use

$$c|_{t=0} = 0 \tag{19}$$

As for the boundary condition, we first focus on the initial surface where the β-phase is in contact with the α-phase. We assume that this surface is described by $\mathbf{X} = \mathbf{X}_h$. As described in Section 2, the β–α interface exits only at $t=0$. As time progresses, the γ-phase is developed between the β-phase and the α-phase, which forms two new interfaces, the β–γ and the γ–α interfaces. In the Lagrangian description, the β–γ interface evolves with time, while the γ–α interface remains at $\mathbf{X} = \mathbf{X}_h$. Evolution of β–γ interface is not known a priori. It needs to be part of the solution to the boundary/initial value problem which will be discussed in the next section. At the γ–α interface, boundary conditions at any current time can be prescribed. Usually, either the concentration or the flux of species A can be is given at the γ–α interfaces, i.e.,

$$c(\mathbf{X}_h,t) = c_0 \quad \text{or} \quad \mathbf{J}(\mathbf{X}_h,t) = \det(\mathbf{F}_\gamma)\mathbf{F}_\gamma^{-1}\mathbf{J}_0, \quad \text{if} \quad \mathbf{X} = \mathbf{X}_h, \tag{20}$$

where $\mathbf{J}_0$ is the prescribed boundary flux in the current state, which may depend on the molar fraction c, as used in the example later in this paper. Note that the term $\det(\mathbf{F}_\gamma)\mathbf{F}_\gamma^{-1}$ is adopted here to transform the current unit area to the initial unit area.

5. Interfacial chemical reaction

For convenience, we introduce the following Eulerian molar concentrations

$$\hat{\rho}_A = \frac{\rho_A}{J_\gamma}, \quad \hat{\rho}_P = \frac{\rho_P}{J_\gamma} \text{ in } \gamma\text{-phase}, \tag{21}$$

$$\hat{\rho}_B = \frac{\rho_B}{J_\beta} \text{ in } \beta\text{-phase}, \tag{22}$$

where J_γ and J_β are the deformation Jacobian of the current γ-phase and β-phase, respectively, i.e.,

$$J_\gamma = \det(\mathbf{F}_\gamma), \quad J_\beta = \det(\mathbf{F}_\beta) \tag{23}$$

Next, let the β–γ interface be described by $\mathbf{X} = \mathbf{X}_s$, and R_s denote the moles of the product $\mathrm{A}_{x_0}\mathrm{B}$ produced per current unit area per unit time at the interface, or rate of production (in moles) of the product $\mathrm{P} = \mathrm{A}_{x_0}\mathrm{B}$ per current unit area. Then, R_s can be written as (Yang, 2010; Zhou et al., 2010)

$$R_s = k_f\left(\hat{\rho}_{\mathrm{A}} - \frac{x_0}{J_\gamma V_m^B}\right)^p (\hat{\rho}_{\mathrm{B}})^q - k_b(\hat{\rho}_{\mathrm{P}})^r \text{ for } \mathbf{X} = \mathbf{X}_s \tag{24}$$

where k_f and k_b are, respectively, the rate constants for the forward and backward reactions described by (1), and $p+q$ and r are the orders of the forward and backward interfacial chemical reactions, respectively. These parameters are material properties and are usually determined experimentally (Chandrasekaran et al., 2010). We note that in order to ensure the spontaneous forward reaction, the molar concentration of species A, i.e., $\hat{\rho}_{\mathrm{A}}$ should be greater than a threshold value $x_0/J_\gamma V_m^B$, where x_0 is the minimum molar fraction needed to form the γ-phase $\mathrm{A}_{x_0}\mathrm{B}$. All the molar concentrations, i.e.,$\hat{\rho}_{\mathrm{A}}$, $\hat{\rho}_{\mathrm{B}}$ and $\hat{\rho}_{\mathrm{P}}$ in (24) are evaluated at the β–γ interface. Since they may not be continuous across the interface, we assume that $\hat{\rho}_{\mathrm{B}}$ is evaluated at the $\beta-$phase side, while $\hat{\rho}_{\mathrm{A}}$ and $\hat{\rho}_{\mathrm{P}}$ are evaluated at the γ-phase side of the β–γ interface.

Making use of (9) and (21)—(22) in (24) leads to

$$R_s = k_f^e \overline{R}_s(c_s), \tag{25}$$

where

$$\overline{R}_s(c_s) = \left.\left(\frac{(x_{\max}c_s - x_0)^p}{\left(J_\gamma\right)^p\left(J_\beta\right)^q} - \frac{k_b^e}{k_f^e\left(J_\gamma\right)^r}\right)\right|_{\mathbf{X}=\mathbf{X}_s} \tag{26}$$

is a dimensionless function, and $k_f^e = k_f/\left(V_m^{\mathrm{B}}\right)^{p+q}$ and $k_b^e = k_b/\left(V_m^{\mathrm{B}}\right)^r$ can be viewed as the effective forward and backward

rate constants, respectively, with the dimension of moles/(area × time). The notation c_s denotes the molar fraction c evaluated on the γ-phase side of the β–γ interface.

If ds and dS denote the elemental areas in the Eulerian and the Lagrangian descriptions, respectively, and $\mathbf{n}$ and $\mathbf{N}$ are their corresponding unit normal vectors, then (Malvern, 1969)

$$\det(\mathbf{F})\mathbf{N}dS = \mathbf{F}^T\mathbf{n}ds \tag{27}$$

Making use of the above, one can show that

$$R_S = \frac{J_\beta R_s}{\sqrt{\mathbf{N}^T\mathbf{F}_\beta^T\mathbf{F}_\beta\mathbf{N}}}, \tag{28}$$

where R_S is the rate of interfacial chemical reaction in the Lagrangian description, i.e., moles of $\mathrm{P}=\mathrm{A}_{x_0}\mathrm{B}$ produced per unit time per unit Lagrangian area.

A continuity equation can then be established by considering the molar conservation of species A at the β–γ interface. On the one hand, the number of moles of species A arriving at the β–γ interface per unit time over a Lagrangian area dS with unit normal $\mathbf{N}$ is $\mathbf{JN}dS$. On the other hand, $R_S dS$ moles of the product $\mathrm{P}=\mathrm{A}_{x_0}\mathrm{B}$ are produced at the β–γ interface per unit time over the area dS, which would consume $x_0 R_S dS$ moles of species A. Therefore, conservation of species A at the β–γ interface requires

$$\mathbf{JN} = -x_0 R_S \ \ for \ \ \mathbf{X} = \mathbf{X}_s, \tag{29}$$

where a negative sign is used because the flux given by (13) is towards the β–γ interface from the γ-phase.

Yet, another continuity equation can be derived by considering the conservation of species B at the β–γ interface. We note that the production of $R_S dSdt$ moles of $\mathrm{P}=\mathrm{A}_{x_0}\mathrm{B}$ will consume $R_S dSdt$ moles of species B, which would reduce the volume of the β-phase by $V_m^B R_S dSdt$. This infinitesimal volume element is a prism with cross-section area dS. Its axis is normal to the β–γ interface, and its length is $V_m^B R_S dt$. To accommodate this volume reduction, the β–γ interface will need to move into the β-phase in the direction normal to the interface by an amount equal to the length of the prism $V_m^B R_S dt$. Therefore, the speed of the β–γ interface in its normal direction is given by,

$$V_N = -V_m^B R_S, \quad for \quad \mathbf{X} = \mathbf{X}_s, \tag{30}$$

where, again, a negative sign is added because the flux given by (13) is towards the β–γ interface from the γ-phase.

Before moving to the next section, we note that the location of the current β–γ interface is generally not known a priori. To fully determine the interface, we assume that, without loss of generality, the β–γ interface is described by

$$f(\mathbf{X}_s,t) = 0, \tag{31}$$

where $f(\mathbf{X}_s,t)$ is a smooth function of $\mathbf{X}_s$ and t. It can be shown (Katardjiev et al., 1994) that $f(\mathbf{X}_s,t)$ must satisfy the following partial differential equation

$$\frac{\partial f(\mathbf{X}_s,t)}{\partial t} + V_N \frac{\Delta f(\mathbf{X}_s,t)}{|\nabla f(\mathbf{X}_s,t)|} = 0, \tag{32}$$

where V_N is the velocity of the β–γ interface in the direction normal to the interface as introduced in (30). Substitution of (30) into (32) yields

$$\frac{\partial f(\mathbf{X}_s,t)}{\partial t} - V_m^B R_S \frac{\Delta f(\mathbf{X}_s,t)}{|\nabla f(\mathbf{X}_s,t)|} = 0, \tag{33}$$

In order to solve (32) for $f(\mathbf{X}_s,t)$, initial conditions are needed. In this case, we assume that the β–α interface at the initial time ($t=0$) is given by the initial β–α interface, i.e., $\mathbf{X}=\mathbf{X}_h$, as discussed in Section 4. Therefore, the initial condition for $f(\mathbf{X}_s,t)$ is

$$f(\mathbf{X}_h,0) = 0 \tag{34}$$

6. Boundary and initial value problem

In summary, the problem posed in Section 1 involves solving the three components of the displacement vector $\mathbf{U}(\mathbf{X},t)$, and the molar fraction of species A in the γ-phase $c(\mathbf{X},t)$. These field quantities could be obtained by solving the three equilibrium Eq. (7), and the diffusion Eq. (18) together with the boundary and initial conditions (8), (19) and (20), if only the location of the β–γ interface $\mathbf{X}=\mathbf{X}_s$ is known as a function of time.

The evolution of the β–γ interface is dictated by two factors, namely, the chemical kinetics, or the rate of chemical reaction at the interface, and the kinematics of the interface. The former is governed by (29) and latter is governed by (33). Solution of these two equations together with the initial condition (34) gives the location of the β–γ interface.

Obviously, all the governing equations mentioned in the last two paragraphs are coupled in one way or the other. Therefore, they must be solved simultaneously. Analytical solution to this nonlinear moving boundary problem system is rather challenging. In what follows, an example will be given and the solutions are obtained numerically.

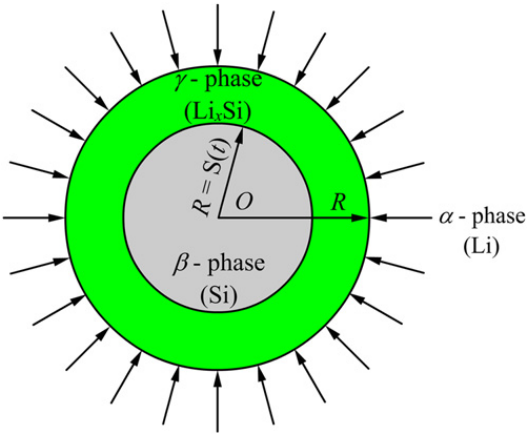

Fig. 2. Schematic of the reaction at a moving boundary during lithiation into a Si pristine particle.

7. Lithiation of a spherical silicon particle

As an example to illustrate the use of the above formulation, we consider the lithiation of a spherical crystal silicon (Si) particle with initial radius R_0. A Lagrangian spherical coordinate system (R,Θ,Φ) is set up so that the origin of the Si is located at $R=0$ at the initial time $t=0$, see Fig. 2. This Si particle is immersed in a liquid electrolyte that contains sufficient lithium ions Li^+. Under the driving force of an electrical current, Li ions in the electrolyte enter into the Si particle at its surface $R=R_0$ through a complex electrochemistry process. Upon entering into the Si particle, Li^+ are reduced into Li. The Li atoms then diffuse into the inside of the Si particle to form the Li_xSi alloy which is typically amorphous. Experimental observations (Limthongkul et al., 2003) and theoretical analyses (Wan et al., 2010; Zhang et al., 2010; Zhao et al., 2011) have shown that a minimum value of $x_0 \approx 0.2$ must be reached in order to form an amorphous $Li_{x_0}Si$ alloy. Once this threshold value is reached, additional Li atoms can diffuse rapidly in the $Li_{x_0}Si$ alloy. This allows the accumulation of more Li atoms at the interface between the crystalline Si and the $Li_{x_0}Si$ alloy, which sustains further reaction to form more $Li_{x_0}Si$ alloy, and moves the interface towards the center of the Si particle. Our objectives are to find (1) the velocity of the interface between the crystalline Si and the Li_xSi alloy, (2) the spatial and temporal distribution of Li in the Li_xSi alloy, and (3) the stresses and strains in both phases.

To use the theory developed in previous sections, we identify the crystalline Si as the β-phase, and the $Li_{x_0}Si$ as the γ-phase, so that Si atoms are species B and Li atoms are species A. The interfacial chemical reaction product is $P=Li_{x_0}Si$. We can now specialize the equations in the previous sections to the problem of lithiation of a spherical Si particle. For simplicity, we assume that all material properties and boundary/initial conditions are isotropic so that the problem is spherically symmetric, and all field quantities are independent of Θ and Φ. For example, the molar fraction of Li in Li_xSi can be written as $c=c(R,t)$, the only non-zero component of the displacement vector is $u_R=u(R,t)$, the only non-zero flux of Li in Li_xSi is $J_R=J_R(R,t)$, and the β–γ interface remains spherical and is given by $R=S(t)$, etc.

Now, let us first consider kinematics of the deformation. Because of the spherical symmetry, the total displacement gradient tensor defined in (3) can be simplified to

$$\mathbf{F}=\langle F_{11},F_{22},F_{33}\rangle=\langle 1+\partial u/\partial R,1+u/R,1+u/R\rangle, \tag{35}$$

where the brackets stands for the diagonal of a matrix. As usual, assume that eigen-transformation due to lithiation is isotropic and given by

$$\mathbf{F}^c=(J^c)^{1/3}\mathbf{I},\ J^c=1+3\eta x_{\max}c, \tag{36}$$

where $x_{\max}=4.4$ represents the saturation concentration of Li in Li_xSi, and η is the coefficient of compositional expansion (CCE) (Swaminathan et al., 2007a,b; Cui et al., 2011). If the plastic deformation is assumed incompressible, i.e., $\det(\mathbf{F}^p)=1$, one can write

$$\mathbf{F}^p=\left\langle \lambda_p,1/\sqrt{\lambda_p},1/\sqrt{\lambda_p}\right\rangle, \tag{37}$$

where λ_p is the plastic stretch in the radial direction. Combining (35)–(37) leads to

$$\mathbf{F}^e=\mathbf{F}(\mathbf{F}^c\mathbf{F}^p)^{-1}=(J^c)^{-1/3}\left\langle\frac{1+\partial u/\partial R}{\lambda_p},(1+u/R)\sqrt{\lambda_p},(1+u/R)\sqrt{\lambda_p}\right\rangle, \tag{38}$$

Making use of (38) gives the elastic strain,

$$\mathbf{E}^e=\frac{1}{2}\left[(\mathbf{F}^e)^T\mathbf{F}^e-\mathbf{I}\right]=\langle E^e_R,E^e_\Theta,E^e_\Phi\rangle \tag{39}$$

Next, we assume that the elastic deformation behavior is governed by

$$\boldsymbol{\sigma}^0 \equiv \frac{\partial W}{\partial \mathbf{F}} = \frac{\partial W}{\partial \mathbf{E}^e}\frac{\partial \mathbf{E}^e}{\partial \mathbf{F}^e}\frac{\partial \mathbf{F}^e}{\partial \mathbf{F}} = \frac{\partial W}{\partial \mathbf{E}^e}\mathbf{F}^e\left(\mathbf{F}^p\right)^{-1}\left(\mathbf{F}^c\right)^{-1}, \tag{40}$$

where $\boldsymbol{\sigma}^0$ is the first P–K stress, and W is the elastic strain energy density in the Lagrangian description,

$$W(\mathbf{F},c) = \frac{J^c}{2}\frac{E(c)}{(1+\nu)}\left(\frac{\nu}{1-2\nu}[tr(\mathbf{E}^e)]^2 + tr\left(\mathbf{E}^e\mathbf{E}^e\right)\right) \tag{41}$$

In the above, $E(c)$ and ν are, respectively, the Young's modulus and Poisson's ratio of the Li_xSi alloy given by

$$E(c) = E_0\left(1+\eta_E x_{\max} c\right), \qquad \nu = \nu_0, \tag{42}$$

where E_0 and ν_0 are the elastic properties of pure amorphous Si. The parameter η_E represents the variation of the Young's modulus with respect to Li concentration c. Making use of (41) in (40) yields the non-zero components of $\boldsymbol{\sigma}^0$,

$$\sigma^0_R = \frac{J^c E(c)}{(1+\nu)(1-2\nu)}\left[(1-\nu)E^e_R + 2\nu E^e_\Theta\right]\frac{2E^e_R+1}{1+\partial u/\partial R}, \tag{43}$$

$$\sigma^0_\Theta = \sigma^0_\Phi = \frac{J^c E(c)}{(1+\nu)(1-2\nu)}\left(\nu E^e_R + E^e_\Theta\right)\frac{2E^e_\Theta+1}{1+u/R} \tag{44}$$

Components of the corresponding Cauchy stress $\boldsymbol{\sigma} = J^{-1}\mathbf{F}\boldsymbol{\sigma}^0$ are given by

$$\sigma_R = \frac{E(c)}{(1+\nu)(1-2\nu)}\left[(1-\nu)E^e_R + 2\nu E^e_\Theta\right]\frac{\sqrt{1+2E^e_R}}{1+2E^e_\Theta}, \tag{45}$$

$$\sigma_\Theta = \sigma_\Phi = \frac{E(c)}{(1+\nu)(1-2\nu)}\left(\nu E^e_R + E^e_\Theta\right)\frac{1}{\sqrt{1+2E^e_R}} \tag{46}$$

Finally, we assume that the viscoplastic behavior of the amorphous Li_xSi alloy is described by the following constitutive equation,

$$\mathbf{D}^p = \frac{\partial G(\sigma_{\text{eff}})}{\partial \boldsymbol{\tau}}, \tag{47}$$

where

$$\mathbf{D}^p = \dot{\mathbf{F}}^p\left(\mathbf{F}^p\right)^{-1} = \frac{\dot{\lambda}_p}{2\lambda_p}\langle 2,-1,-1\rangle \tag{48}$$

is the rate of plastic deformation tensor, and

$$\sigma_{\text{eff}} = \sqrt{\frac{3}{2}}\sqrt{tr\left[\left(\boldsymbol{\sigma}-\frac{tr(\boldsymbol{\sigma})}{3}\mathbf{I}\right)\left(\boldsymbol{\sigma}-\frac{tr(\boldsymbol{\sigma})}{3}\mathbf{I}\right)\right]}, \tag{49}$$

is the effective Cauchy stress, and $G(\sigma_{\text{eff}})$ is the flow potential. Following our previous work (Cui et al., 2012b), we adopt the following power-law form for the flow potential

$$G(\sigma_{\text{eff}}) = \frac{\sigma_f \dot{d}_0}{m+1}\left(\frac{\sigma_{\text{eff}}}{\sigma_f}-1\right)^{m+1} H\left(\frac{\sigma_{\text{eff}}}{\sigma_f}-1\right), \tag{50}$$

where $H(x)$ is the Heaviside step function, σ_f, $\dot{d}_0$ and m are material constants, which may depend on the Li concentration. Clearly, σ_f is the unidirectional yield (Cauchy) strength, $\dot{d}_0$ is the reciprocal of viscosity and m is the stress exponent ($m=1$ yields viscoelastic behavior). We note that this is a slightly modified version of the one used by Bower et al. (2011). The modification is to ensure a smooth transition from the elastic to the plastic regimes. The material constants σ_f, $\dot{d}_0$ and m used in the numerical simulations are listed in Table 1. It was derived in Cui et al. (2012b) that the above viscoplastic law leads to

$$\frac{\dot{\lambda}_p}{\lambda_p} = \text{sgn}(\sigma_R-\sigma_\Theta)\dot{d}_0\left(\frac{\sigma_{\text{eff}}}{\sigma_f}-1\right)^m H\left(\frac{\sigma_{\text{eff}}}{\sigma_f}-1\right) \tag{51}$$

This completes the set of equations for the kinematics of the deformation in the Li_xSi alloy. Observation of these equations reveals that all the field quantities such as the elastic strain $\mathbf{E}^e$, the P–K stress $\boldsymbol{\sigma}^0$ and the plastic stretch λ_p are functions of the displacement $u_R = u(R,t)$. In other words, once $u(R,t)$ is known, $\mathbf{E}^e$ can be calculated from (39). Consequently, $\boldsymbol{\sigma}^0$ can be calculated from (43) and (44), and λ_p can be solved from (51). Of course, these equations are coupled, thus must be solved simultaneously.

A caveat needs to be inserted here. All the equations above were derived for the Li_xSi alloys. Therefore, they are valid only for $S(t) < R < R_0$, where $S(t)$ is the location of the interface between the crystalline Si and the amorphous Li_xSi.

Table 1
Material properties and initial parameters used in our model.

A_0 parameters of the activity constant	−0.3063 eV/atom
B_0 parameters of the activity constant	−0.4003 eV/atom
D_0 diffusivity of Si anode	1×10^{-13} m^2/s [d]
$\dot{\bar{d}}_0$ normalized characteristic strain rate for plastic flow in Li_xSi	0.4
E_0 elastic constant of pure silicon	166 GPa (crystalline) 90.13 GPa (amorphous)[a]
m stress exponent for plastic flow in Si	4 [b]
R_g gas constant	8.314 J K^{-1}/mol
T temperature	300 K
V_m^B molar volume of Si	1.2052×10^{-5} m^3/mol
x_{max} maximum concentration	4.4
α coefficient of diffusivity	0.18[c]
η coefficient of compositional expansion (CCE)	0.2356
η_E rate of change of elastic modulus with concentration	−0.1464[a]
v_0 Poisson's ratio of Si electrode	0.22 (crystalline) 0.28 (amorphous)
σ_f initial yield stress of Si	0.12 GPa[b]
p reaction order of reactant A (Li)	1
q reaction order of reactant B (Si)	0.5
$\bar{J}_0$ prescribed flux at the boundary	0.1

[a] Rhodes et al. (2010).
[b] Bower et al. (2011).
[c] Haftbaradaran et al. (2011).
[d] Cui et al. (2012a).

However, these equations can still be used for $0\le R<S(t)$ if

$$c(R,t)\equiv 0,\ \ \lambda_p(R,t)\equiv 1 \tag{52}$$

are used. So, in the rest of this paper, will implicitly assume that (52) holds for all field quantities in the crystalline Si, i.e., $0\le R<S(t)$. Of course, the elastic modulus and Poisson's ratio should be the ones for pure crystalline Si, which are also given in Table 1.

To determine $u(R,t)$, we turn our attention to mechanical equilibrium. Due to spherical symmetry, the only non-zero stress components are σ_R^0, and $\sigma_\Theta^0=\sigma_\Phi^0$, and the equation of equilibrium (7) reduces to

$$\frac{\partial\sigma_R^0}{\partial R}+2\frac{\sigma_R^0-\sigma_\Theta^0}{R}=0 \tag{53}$$

By neglecting the hydrostatic pressure from the liquid electrolyte, the Si particle surface can be treated as traction-free, i.e.,

$$\sigma_R(R_0,t)=0 \tag{54}$$

At the interface $R=S(t)$, we assume the continuity of displacement and traction, i.e.,

$$\lim_{R\to S^-(t)}u(R,t)=\lim_{R\to S^+(t)}u(R,t),\qquad \lim_{R\to S^-(t)}\sigma_R(R,t)=\lim_{R\to S^+(t)}\sigma_R(R,t), \tag{55}$$

where $S^-(t)$ and $S^+(t)$ means approaching $S(t)$ from the Si side and from the Li_xSi side, respectively. Making use of (43) and (44) in (53)–(55) results in a boundary value problem for $u(R,t)$ in $0\le R<R_0$. However, solution of this boundary value problem is not possible yet, because it contains $c=c(R,t)$, i.e., molar fraction of Li in Li_xSi, which is an unknown in $S(t)<R<R_0$ at this point.

To determine $c=c(R,t)$ in $S(t)<R<R_0$, the continuity Eq. (18) will be needed. For the particular case considered here, Eq. (18) is simplified to

$$\frac{x_{max}\partial c}{V_m^B\partial t}+\frac{\partial J_R}{\partial R}+\frac{2J_R}{R}=0,\qquad for\qquad S(t)<R<R_0 \tag{56}$$

where

$$J_R=-\frac{1}{R_gT}\frac{x_{max}c}{V_m^B}\frac{D}{F_{11}^2}\frac{\partial\mu(\mathbf{F},c)}{\partial R}, \tag{57}$$

is the only non-zero component of the Li flux, D is the diffusivity of Li in the Li_xSi alloy, which may be stress and concentration dependent, and $\mu(\mathbf{F},c)$ is the stress-dependent chemical potential introduced in (11).

The initial conditions at $t=0$ can be specified as

$$c(R,0)=0 \tag{58}$$

At the boundary $R=R_0$, we specify the flux of Li enters the Si particle as

$$J_R=J_0(1+u/R)^2[1-c], \quad for \quad R=R_0, \tag{59}$$

where J_0 is a constant representing the charging rate in the current state. It can be seen shown (Chen et al., 2009) that (59) is a linearized form of the Butler–Volmer equation. At the interface $R=S(t)$, the continuity Eq. (29) is needed, which for the example considered here reduces to

$$J_R=-x_0(1+u/R)^2R_s, \quad for \quad R=S^+(t), \tag{60}$$

where R_s is the chemical reaction rate at the interface in the current state, see (24).

Since all field quantities in (56)–(60) can be expressed as functions of $c(R,t)$, these equations form an initial/boundary value problem for $c(R,t)$. To solve this initial/boundary value problem, one will need to know $S(t)$. The equation for governing $S(t)$ is given by (30), which for the example at hand simplifies to

$$V_N=\dot{S}(t)=-V_m^B(1+u/R)^2R_s \quad for \quad R=S^-(t) \tag{61}$$

The initial condition for the above is

$$S(0)=R_0 \tag{62}$$

Now, let us summarize the above discussions. There are three unknown quantities of interest, $u_R=u(R,t)$, $c=c(R,t)$ H$(R-S(t))$, and $S(t)$. In principle, $u_R=u(R,t)$ can be obtained from solving the boundary value problem (53)–(55), $c(R,t)$ can be obtained from solving (56)–(59), and $S(t)$ can be obtained from solving (61) and (62), albeit these equations are coupled. Although this system of coupled equation can be solved analytically (Cui et al., 2012c) under certain simplifying assumptions, numerical solutions are needed for the general case. In the current study, the commercial software COMSOL was used for this purpose. The results are presented below.

To facilitate the numerical computations, the following non-dimensional variables are introduced,

$$\overline{R}=\frac{R}{R_0}, \quad \overline{D}=\frac{D}{D_0}, \quad \overline{t}=\frac{D_0t}{R_0^2}, \quad \overline{u}=\frac{u}{R_0}, \quad \overline{S}=\frac{S}{R_0} \tag{63}$$

$$\overline{J}_0=\frac{V_m^BR_0J_0}{D_0x_{\max}}, \quad \overline{\dot{d}_0}=\frac{R_0^2}{D_0}\dot{d}_0 \tag{64}$$

where D_0 is a constant representing the diffusion coefficient of Li in amorphous Si in a stress-free state. For convenience, we list below some of the relevant equations in terms of the dimensionless variables.

$$\frac{\partial\sigma_R^0}{\partial\overline{R}}+2\frac{\sigma_R^0-\sigma_\Theta^0}{\overline{R}}=0 \quad for \quad 0<\overline{R}<1 \tag{65}$$

$$\frac{\partial c}{\partial\overline{t}}=\frac{\partial}{\partial\overline{R}}\left(\frac{\overline{D}c}{F_{11}^2}\frac{\partial\mu}{R_gT\partial\overline{R}}\right)+\frac{2}{\overline{R}}\left(\frac{\overline{D}c}{F_{11}^2}\frac{\partial\mu}{R_gT\partial\overline{R}}\right), \quad for \quad \overline{S}(\overline{t})<\overline{R}<1, \tag{66}$$

$$-\frac{\overline{D}c}{F_{11}^2}\frac{\partial\mu}{R_gT\partial\overline{R}}=\overline{J}_0(1+\overline{u})^2[1-c], \quad for \quad \overline{R}=1 \tag{67}$$

$$\frac{1}{R_gT}\frac{\overline{D}}{F_{11}^2}c\frac{\partial\mu(\mathbf{F},c)}{\partial\overline{R}}=\beta\frac{x_0}{x_{\max}}\left(1+\frac{\overline{u}}{\overline{R}}\right)^2\overline{R}_s(c^+), \quad for \quad R=S^+(t) \tag{68}$$

$$\overline{V}(\overline{t})\equiv\frac{d\overline{S}}{d\overline{t}}=-\beta\left(1+\frac{\overline{u}}{\overline{R}}\right)^2\overline{R}_s(c^+), \quad for \quad R=S^-(t), \tag{69}$$

where

$$\beta=k_f^eV_m^BR_0/D_0 \tag{70}$$

is a dimensionless parameter that is analogous to the well-known Biot number in heat transfer. It is seen that β is a measure of the relative rates between the chemical reaction at the Si–Li_xSi interface and the diffusion of Li in the Li_xSi. The significance of β will be discussed later.

In our numerical calculations, the activity constant and the diffusivity are assumed to depend on Li concentration according to the followings Haftbaradaran et al. (2011),

$$\gamma=\frac{1}{1-c}\exp\left(\frac{1}{R_gT}\left[2(A_0-2B_0)c-3(A_0-B_0)c^2\right]\right), \tag{71}$$

$$D=D_0\overline{D}\equiv D_0\exp\left(\frac{\alpha V_m^B\sigma_\Theta^0}{R_gT}\right), \tag{72}$$

where the parameters A_0 and B_0 can be derived from the mixing enthalpy of Li_xSi by using the first-principles calculations (Shenoy et al., 2010). All the constants and other materials properties required in the numerical calculations are listed in Table 1.

8. Results and discussions

Shown in Fig. 3 is the Li concentration profile as a function of charging time. Results for different values of β are plotted. The first thing observed from these plots is the sharp interface between the crystalline Si and the amorphous Li_xSi alloy which creates the core/shell structure often observed in the lithiation of Si nanowires and nanoparticles (Chan et al., 2008; Liu and Huang, 2011). It is also seen that for small β, the Si/Li_xSi interface moves very slowly, and the Li distribution is uniform in the alloy, and reaches its saturation concentration $c=1$. For larger β, the interface moves faster, and the Li distribution becomes non- uniform in the alloy. These results can be understood by recalling that $\beta=k_f^e V_m^B R_0/D_0$, see (70). Therefore, for a fixed particle size R_0, very small β means that the interfacial chemical reaction rate k_f^e is much lower than the diffusion rate D_0 of Li in Si. In this case, the Si/Li_xSi interface would move very slowly in comparison to the diffusion of Li in the alloy. Thus, Li fills up the alloy quickly. For large β, however, the interfacial chemical reaction is faster, and Li diffuses at a much slower rate. Thus, it cannot fill up the alloy quickly enough so its concentration near the interface becomes lower. In other words, the values of β determines the nature of the diffusion/reaction dynamics. Very small β means that the kinetics of the process is controlled by the chemical reaction at the Si/Li_xSi, while very large β means that the kinetics of process is controlled by the diffusion of Li in the alloy.

To further investigate the transition from reaction to diffusion controlled processes, we plotted the Si/Li_xSi interface velocity as a function of time for different values of β in Fig. 4. It is seen that in all cases, the interface velocity increases initially, reaches a peak value, and eventually slows down drastically. At the moment when the interface velocity reaches its peak value, the amount of Li delivered to the interface by diffusion provides just about the amount of Li needed to sustain enough chemical reaction so that the interface moves in a constant speed. In this case, the two processes, diffusion and chemical reaction are in equilibrium. If the amount of Li delivered to the interface by diffusion is more than what the chemical reaction can consume at a given interface speed, the interface will have to speed up to consume more Li. In this case, the chemical reaction is the slower process so that the overall kinetics is limited by the interfacial chemical reaction. If the amount of Li delivered to the interface is less than the amount needed to sustain the chemical reaction at a given interface speed, the interface will have to slow down. In this case, the diffusion is the slower process, and the overall kinetics is limited by the diffusion. The results in Fig. 4 indicate that the overall kinetics of lithiation of a Si particle is always controlled by the interfacial chemical reaction initially. As the interface moves away from the particle surface, Li atoms need to travel longer distance to reach the interface. Thus, diffusion gradually takes over and eventually becomes the controlling process.

Therefore, the moment $\bar{t}=\bar{t}_c$ where $\bar{t}_c$ satisfies $\overline{V}'(\bar{t}_c)=0$ will be called the transition time. The distance $\bar{L}_c\equiv 1-\bar{S}(\bar{t}_c)$ will be called the transition distance. Since the concentration of Li decreases almost parabolically from its source, the farther away from the source, the lower the Li concentration is. Therefore, $\bar{L}_c$ represents the distance over which Li needs to travel before its concentration is just about to fall below the threshold needed to sustain the interfacial chemical reaction at that given interface speed. The transition distance depends on the ratio between the rate of interfacial chemical reaction and the rate of diffusion of Li. Higher reaction rate tends to decrease the transition distance, and vice versa. In terms of dimensionless variables, $\bar{L}_c$ becomes a function of β. The relationship between $\bar{L}_c$ and β is plotted in Fig. 5. As expected, smaller β, i.e., slower interfacial reaction, requires longer transition distance, and vice versa. In the limit of $\beta\to 0$, the interfacial reaction is so slow that it is always in control. In other words, the diffusion is so fast (in comparison to interfacial chemical reaction) that the Li_xSi alloy is always fully saturated with Li. Thus, the interface will move at a constant speed. In the limit of $\beta\to\infty$, however, the interfacial reaction is so fast that diffusion is always in control. In this case, the problem effectively reduces to the conventional diffusion problem considered in the literature, see, for example, (Cui et al., 2012b).

A trivial algebraic exercise shows that if $\bar{L}_c=0.82$, then over 99% of the original Si particle volume would be lithiated before the interface velocity is slowed down by diffusion. In other words, for any value of $\bar{L}_c>0.82$, the entire lithiation process could be considered as the reaction controlled. We note that the value of the rate of interfacial chemical reaction for Si and Li is not available in the open literature. In a recent study (Chandrasekaran et al., 2010), Chandrasekaran et al. reported a reaction rate constant $k_f=2.5\times 10^{-9}\ \ (\mathrm{m/s})/\sqrt{\mathrm{mol/m^3}}$ for the reaction at the Si/Li_xSi/electrolyte interfaces. Using this value as an approximation for the k_f in our case, and $\bar{L}_c=0.82$ as the transition distance, we found from $\beta=k_f^e V_m^B R_0/D_0$ that $R_0\approx 150$ nm for the parameters given in Table 1. In other words, for Si particles with radii less than 150 nm, the entire lithiation process is controlled by the interfacial reaction. The smaller the particle, the more saturated the Li_xSi is. Recent experimental observations seem to confirm this conclusion, e.g., (Ryu et al., 2011; Lee et al., 2012; Liu et al., 2012).

Further, if one take $R_0=150$ nm as the initial Si particle size. Then using the above k_f value and other parameters specified in Table 1, one can estimate that $\beta=1.0$. For this value of β, it is seen from Fig. 4 that over a long time period, the interface velocity is approximately a constants $\overline{V}_N\approx 0.80$, which corresponds to the physical velocity of the interface $V_N\approx 500\ nm/s$. This value is higher than the reported experimental measurements ($\sim$100 nm/s) on Si nanowires

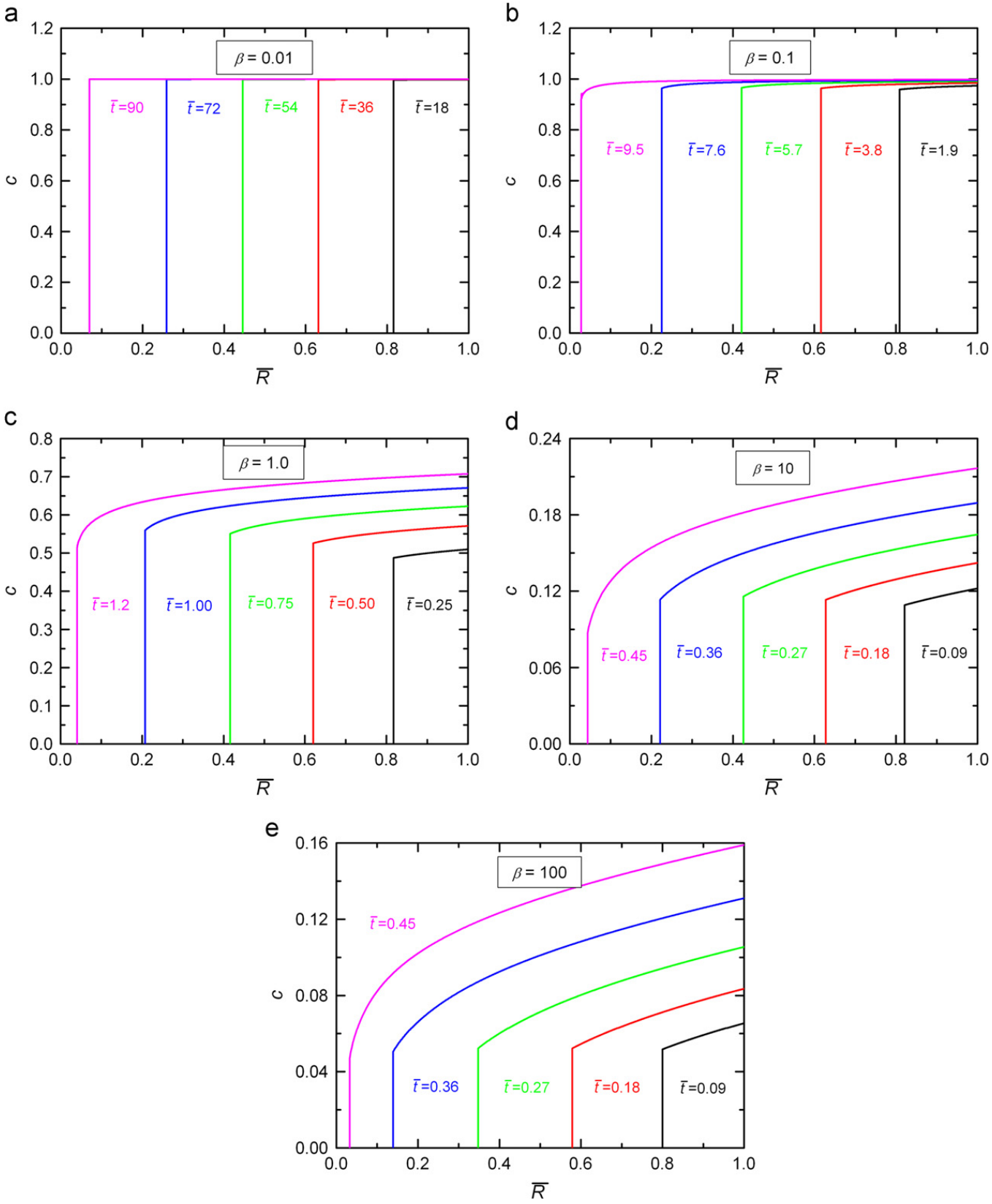

Fig. 3. Distribution of Li concentration at different time for (a) β=0.01; (b) β=0.1; (c) β=1; (d) β=10; (e) β=100.

(Liu et al., 2011). The reasons could be several including the values of k_f and D_0 used in the calculations, as well as the higher Li flux prescribed at electrode/electrolyte interface.

By integrating the interface velocity, the thickness of the lithiated region $1-\bar{S}(\bar{t})$ can be computed as a function of t. Results for different values of β are shown in Fig. 6. It is seen that the thickness of the lithiated shell region grows linearly

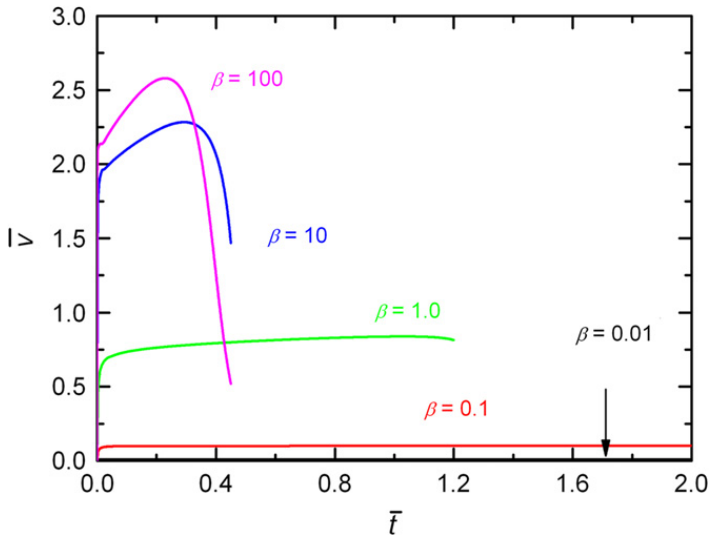

Fig. 4. Interface velocity as a function of time for various values of β.

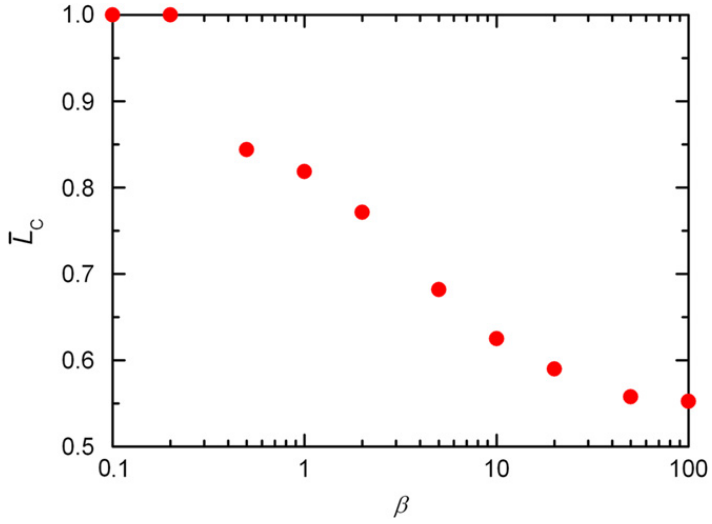

Fig. 5. Transition distance $\bar{L}_c$ versus β.

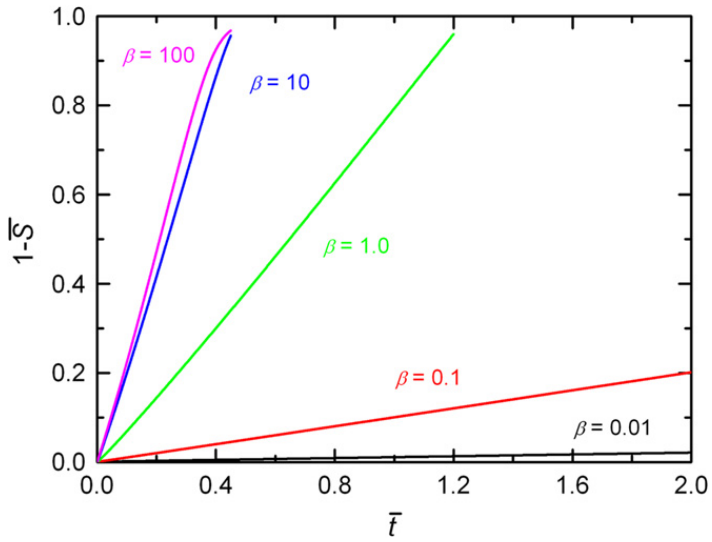

Fig. 6. Thickness of the lithiated shell-region for different values of β.

with t, as expected for the case of first order chemical reaction $p=1$. For large β, the growth rate is initially linear when the process is controlled by the interfacial chemical reaction. Beyond the transition length $\bar{L}_c$, the lithiation process becomes diffusion controlled. Thus, the thickness growth shows the typical parabolic dependence on time. Obviously, in the case of $\beta\to\infty$, the entire growth is parabolic.

Let us now turn our attention to the stress. Due to spherical symmetry, the only non-zero stress components are the radial stress σ_R and the hoop stress σ_Θ. Since deformation remains elastic, it can be shown that $\sigma_R=\sigma_\Theta=$ const. in the unlithiated region. Figs. 7 and 8 plot the evolution of stresses σ_R and σ_Θ for different values of β. As expected, the

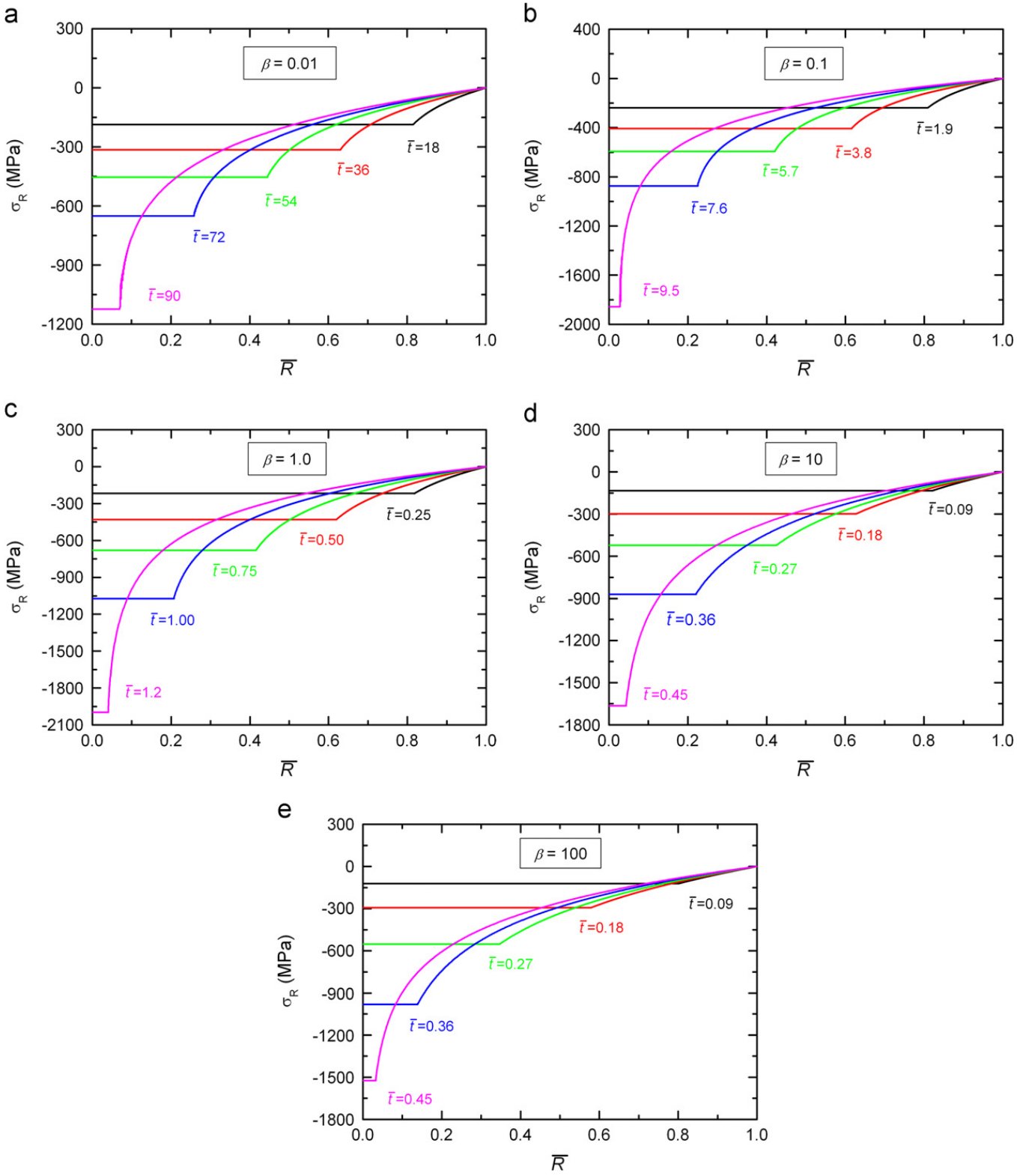

Fig. 7. Distribution radial stress σ_R at different time for (a) $\beta=0.01$; (b) $\beta=0.1$; (c) $\beta=1$; (d) $\beta=10$; (e) $\beta=100$.

unlithiated Si core is under a uniform hydrostatic pressure during charging. This hydrostatic pressure increases monotonically as the Si–Li_xSi interface moves toward the particle center. Throughout the entire particle, the radial stress σ_R is always negative and approaches to zero at the surface. The hoop stress σ_Θ is negative towards the particle center, and positive towards the particle surface. Such positive hoop stress is due to the spherical geometry of the particle and the viscoplastic behavior of the Li_xSi alloy. Another observation is $\beta=1$ seems to give the highest stress field. This might be a result of the viscoplastic nature of the Li_xSi alloy. For $\beta\ll 1$, the interface moves very slowly, so there is plenty of time for the lithiated material to relax so the stress does not go very high. For $\beta\gg 1$, the interface moves very fast, so there is not

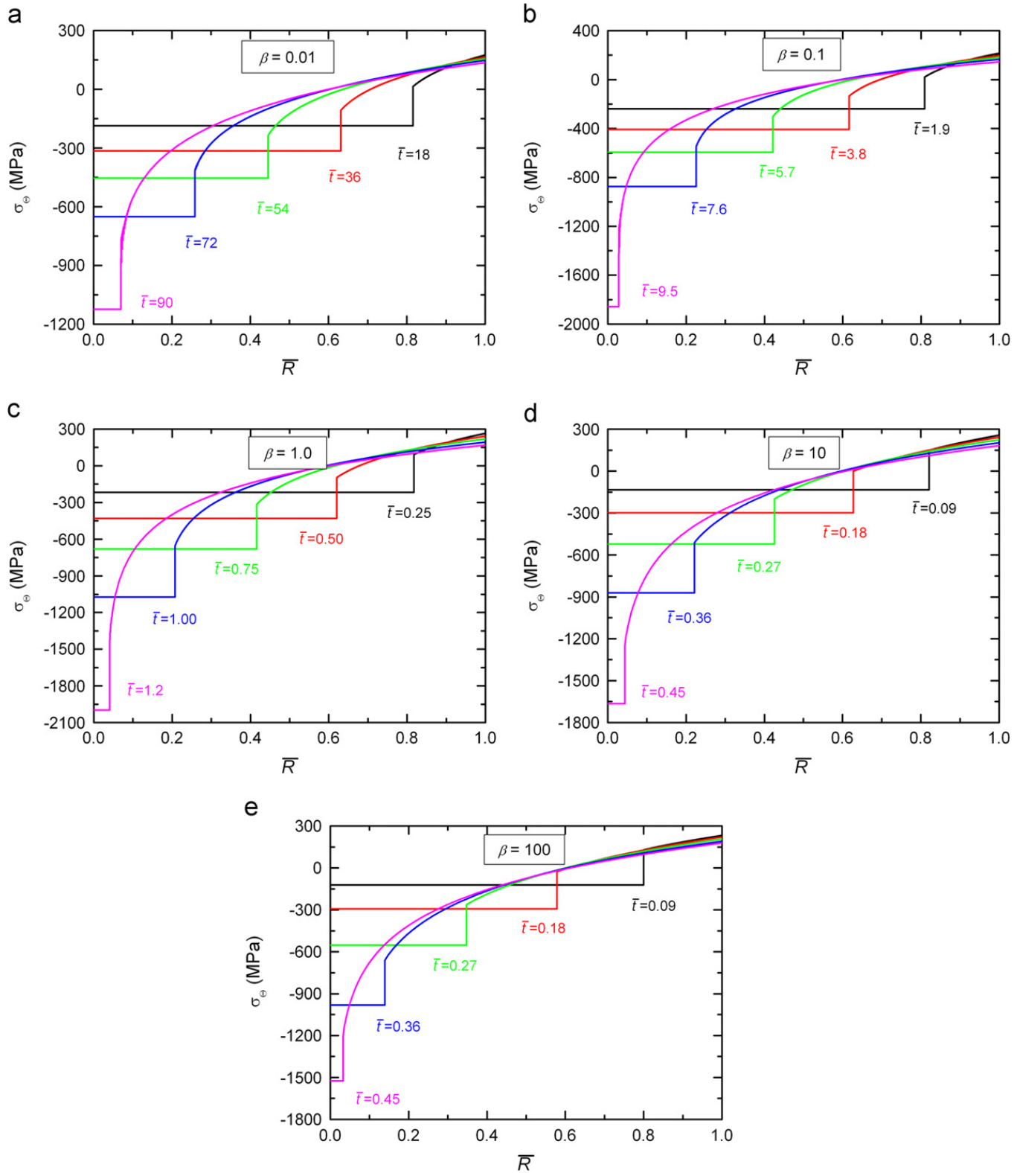

Fig. 8. Distribution of hoop stress σ_Θ at different times for (a) β=0.01; (b) β=0.1; (c) β=1; (d) β=10; (e) β=100.

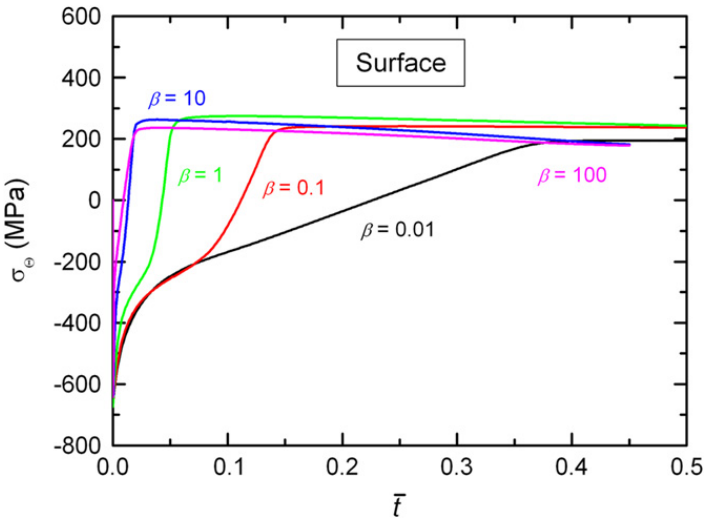

Fig. 9. Evolution of stress σ_Θ at a point on the particle surface.

enough time to build higher Li concentration that hinders the stress build up. When the interface speed and viscoplastic relaxation are in equilibrium, stresses become the highest. This happens around $\beta=1$ for the specific case considered here.

Plotted in Fig. 9 is the hoop stress on the particle surface $R=R_0$ as a function of time. It is seen that σ_Θ is initially compressive as expected. However, very quickly, the hoop stress becomes tensile due to reverse plasticity of the Li_xSi alloy as the Si/Li_xSi interface moves inward. This tensile stress might be the cause of the radial cracks in the particle (Liu and Huang, 2011; Liu et al., 2012). It is seen from Fig. 9 that the maximum tensile stress is insensitive to the Biot parameter β because of plasticity. Nevertheless, the highest hoop stress on the particle surface seem to occur around $\beta=1$. This again illustrates the competition between stress relaxation due to viscoplasticity and stress build up due to Li concentration increase, as explained in the previous paragraph. This also leads to observation that, for smaller (larger) β, the hoop stress takes longer (shorter) time to reach its maximum. This is expected since smaller (larger) β means the entire kinetics of the lithiation process is slower (faster).

Finally, we mention that in the limit of $\beta\to\infty$, the solution presented in this work reduces to that obtained in our previous work (Cui et al., 2012b), where the interfacial chemical reaction rate is assumed infinite.

9. Summary and conclusions

In this work, we developed a mathematical framework to investigate the interaction between bulk diffusion and interfacial chemical reaction in binary systems. The new model accounts for finite deformation kinematics and stress–diffusion interaction. It is applicable to arbitrary shape of the phase interface. As an example, the model is used to study the lithiation of a spherical silicon particle. It is found that a dimensionless parameter $\beta=k_f^e V_m^B R_0/D_0$ plays a significant role in determining the overall kinetics of the lithiation process. This parameter, analogous to the Biot number in heat transfer, represents the ratio of the rate of interfacial chemical reaction and the rate of bulk diffusion. Smaller β means slower interfacial reaction, which would result in higher concentration of lithium in the lithiated region. On the other hand, large β means faster interfacial reaction. In the limit of $\beta\to\infty$, the current solution reduces to that of Cui et al. (2012b) where the interfacial chemical reaction rate is assumed infinite. Our solution shows that the unlithiated and lithiated regions are separated by a sharp interface, resulting in a core–shell structure consistent with experimental observations. This sharp interface moves towards the particle center as lithiation progresses. The interface velocity predicted by our model is comparable to experimental measurements. Furthermore, we found that, for a given β, the lithiation process is always controlled by the interfacial chemical reaction initially, until sufficient silicon has been lithiated so that the diffusion distance for lithium reaches a threshold value, beyond which bulk diffusion becomes the slower process and controls the overall lithiation kinetics.

Our numerical results based on the materials properties available in the literature, show that the entire lithiation process is controlled by interfacial chemical reaction for Si particles with radius less than 150 nm. Our results suggest a strategy to relax the tensile hoop stress on the surface quickly by doping Si with other elements to increase the rate of interfacial chemical reaction.

Acknowledgments

This work was supported in part by an ISEN Booster Award at Northwestern University, and in part by NSF through CMMI-1200075.

References

Abart, R., Petrishcheva, E., 2011. Thermodynamic model for reaction rim growth: interface reaction and diffusion control. Am. J. Sci. 311 (6), 517–527.

Abart, R., Petrishcheva, E., Joachim, B., 2012. Thermodynamic model for growth of reaction rims with lamellar microstructure. Am. Mineral. 97 (1), 231–240.

Ang, W.T., 2008. A numerical method based on integro-differential formulation for solving a one-dimensional Stefan problem. Numer. Methods Part. Differ. Equ. 24 (3), 939–949.

Bower, A.F., Guduru, P.R., Sethuraman, V.A., 2011. A finite strain model of stress, diffusion, plastic flow, and electrochemical reactions in a lithium-ion half-cell. J. Mech. Phys. Solids 59, 804–828.

Caldwell, J., Kwan, Y.Y., 2004. Numerical methods for one-dimensional Stefan problems. Commun. Numer. Methods Eng. 20 (7), 535–545.

Caldwell, J., Kwan, Y.Y., 2009. A brief review of several numerical methods for one-dimensional Stefan problems. Therm. Sci. 13 (2), 61–72.

Chan, C.K., Peng, H.L., Liu, G., McIlwrath, K., Zhang, X.F., Huggins, R.A., Cui, Y., 2008. High-performance lithium battery anodes using silicon nanowires. Nat. Nanotechnol. 3 (1), 31–35.

Chandrasekaran, R., Magasinski, A., Yushin, G., Fuller, T.F., 2010. Analysis of lithium insertion/deinsertion in a silicon electrode particle at room temperature. J. Electrochem. Soc. 157 (10), A1139–A1151.

Chen, C.H., Ding, N., Xu, J., Yao, Y.X., Wegner, G., Fang, X., Lieberwirth, I., 2009. Determination of the diffusion coefficient of lithium ions in nano-Si. Solid State Ionics 180 (2-3), 222–225.

Chon, M.J., Sethuraman, V.A., McCormick, A., Srinivasan, V., Guduru, P.R., 2011. Real-time measurement of stress and damage evolution during initial lithiation of crystalline silicon. Phys. Rev. Lett. 107, 4.

Cui, L.F., Ruffo, R., Chan, C.K., Peng, H.L., Cui, Y., 2009. Crystalline–amorphous core–shell silicon nanowires for high capacity and high current battery electrodes. Nano Lett. 9 (1), 491–495.

Cui, Z.W., Gao, F., Cui, Z.H., Qu, J.M., 2012a. A second nearest-neighbor embedded atom method interatomic potential for Li–Si alloys. J. Power Sources 207, 150–159.

Cui, Z.W., Gao, F., Qu, J.M., 2012b. A finite deformation stress-dependent chemical potential and its applications to lithium ion batteries. J. Mech. Phys. Solids 60 (7), 1280–1295.

Cui, Z.W., Gao, F., Qu, J.M., 2012c. On the perturbation solution of interface-reaction controlled diffusion in solids. Acta Mech. Sin. 28, 1049–1057.

Cui, Z.W., Sun, Y., Chen, Y.J., Qu, J.M., 2011. Semi-ab initio interionic potential for gadolinia-doped ceria. Solid State Ionics 187 (1), 8–18.

Deb, S., Pitchumani, R., 2011. Analysis of nonisothermal sintering of nanocrystalline and microscaled ceramic materials. Adv. Appl. Ceram. 110 (5), 301–310.

Deshpande, R., Cheng, Y.T., Verbrugge, M.W., Timmons, A., 2011. Diffusion induced stresses and strain energy in a phase-transforming spherical electrode particle. J. Electrochem. Soc. 158 (6), A718–A724.

Dybkov, V.I., 2010. Reaction diffusion and solid state chemical kinetics. React. Diffu. Solid State Chem. Kinet. 67-68, 1–312.

Filipek, R. 2005. Modelling of Interdiffusion and Reactions at the Boundary; Initial-Value Problem of Interdiffusion in the Open System. Diffusion in Materials: Dimat 2004, Pts 1 and 2. M. Danielewski, R. Filipek, R. Kozubs et al. 237-240,250-256.

Furuto, A., Kajihara, M., 2008. Numerical analysis for kinetics of reactive diffusion controlled by boundary and volume diffusion in a hypothetical binary system. Mater. Trans. 49 (2), 294–303.

Gotze, L.C., Abart, R., Rybacki, E., Keller, L.M., Petrishcheva, E., Dresen, G., 2010. Reaction rim growth in the system MgO–Al(2)O(3)–SiO(2) under uniaxial stress. Mineral. Petrol. 99 (3-4), 263–277.

Haftbaradaran, H., Song, J., Curtin, W.A., Gao, H.J., 2011. Continuum and atomistic models of strongly coupled diffusion, stress, and solute concentration. J. Power Sources 196 (1), 361–370.

Hou, X.M., Lu, X., Peng, B., Zhao, B.J., Zhang, M., Chou, K.C., 2012. A new approach to interpreting the parabolic and non-parabolic oxidation behaviour of hot-pressed beta-SiAlON ceramics. Corros. Sci. 58, 278–283.

Katardjiev, I.V., Carter, G., Nobes, M.J., Berg, S., Blom, H.O., 1994. Three-dimensional simulation of surface evolution during growth and erosion. J. Vac. Sci. Technol., A: Vac. Surf. Films 12 (1), 61–68.

Lee, S.W., McDowell, M.T., Berla, L.A., Nix, W.D., Cui, Y., 2012. Fracture of crystalline silicon nanopillars during electrochemical lithium insertion. Proc. Nat. Acad. Sci. U.S.A. 109 (11), 4080–4085.

Lee, S.W., McDowell, M.T., Choi, J.W., Cui, Y., 2011. Anomalous shape changes of silicon nanopillars by electrochemical lithiation. Nano Lett. 11 (7), 3034–3039.

Limthongkul, P., Jang, Y.I., Dudney, N.J., Chiang, Y.M., 2003. Electrochemically-driven solid-state amorphization in lithium-metal anodes. J. Power Sources 119, 604–609.

Liu, X.H., Huang, J.Y., 2011. In situ TEM electrochemistry of anode materials in lithium ion batteries. Energy Environ. Sci. 4 (10), 3844–3860.

Liu, X.H., Zhang, L.Q., Zhong, L., Liu, Y., Zheng, H., Wang, J.W., Cho, J.H., Dayeh, S.A., Picraux, S.T., Sullivan, J.P., Mao, S.X., Ye, Z.Z., Huang, J.Y., 2011. Ultrafast electrochemical lithiation of individual Si nanowire anodes. Nano Lett. 11 (6), 2251–2258.

Liu, X.H., Zhong, L., Huang, S., Mao, S.X., Zhu, T., Huang, J.Y., 2012. Size-dependent fracture of silicon nanoparticles during lithiation. ACS Nano 6 (2), 1522–1531.

Malvern, L.E., 1969. Introduction to the Mechanics of a Continuous Medium. Pretice-Hall, London.

Murray, P., Carey, G.F., 1988a. Finite-element analysis of diffusion with reaction at a moving boundary. J. Comput. Phys. 74 (2), 440–455.

Murray, P., Carey, G.F., 1988b. The role of film stress on the rate of silicon oxidation at low-temperature. J. Electrochem. Soc. 135 (8). C376-C376.

Murray, P., Carey, G.F., 1989a. Compressibility effects in modeling thin silicon dioxide film growth. J. Electrochem. Soc. 136 (9), 2666–2673.

Murray, P., Carey, G.F., 1989b. Determination of Interfacial stress during thermal-oxidation of silicon. J. Appl. Phys. 65 (9), 3667–3670.

Murray, P., Carey, G.F., 1990. Viscous-flow and transport with moving free and reactive surfaces. Int. J. Numer. Methods Eng. 30 (6), 1181–1194.

Qian, J.W., Li, J.L., Xiong, J.T., Zhang, F.S., Lin, X., 2011. Study on reaction kinetics in diffusion bonding of Ti2AlNb and GH4169 with Nb+Ni foils as interlayer. Rare Met. Mater. Eng. 40 (12), 2106–2110.

Ramos, J.I., 2005. Exponential numerical methods for one-dimensional one-phase Stefan problems. Arch. Appl. Mech. 74 (10), 664–678.

Reemtsen, R., Kirsch, A., 1984. A method for the numerical-solution of the one-dimensional inverse Stefan problem. Numer. Math. 45 (2), 253–273.

Rhodes, K., Dudney, N., Lara-Curzio, E., Daniel, C., 2010. Understanding the degradation of silicon electrodes for lithium-ion batteries using acoustic emission. J. Electrochem. Soc. 157 (12), A1354–A1360.

Ryu, I., Choi, J.W., Cui, Y., Nix, W.D., 2011. Size-dependent fracture of Si nanowire battery anodes. J. Mech. Phys. Solids 59 (9), 1717–1730.

Shenoy, V.B., Johari, P., Qi, Y., 2010. Elastic softening of amorphous and crystalline Li–Si phases with increasing Li concentration: a first-principles study. J. Power Sources 195 (19), 6825–6830.

Swaminathan, N., Qu, J., 2007. Interactions between non-stoichiometric stresses and defect transport in a tubular electrolyte. Fuel Cells 7 (6), 453–462.

Swaminathan, N., Qu, J., 2009. Evaluation of thermomechanical properties of non-stoichiometric gadolinium doped ceria using atomistic simulations. Modell. Simul. Mater. Sci. Eng. 17 (4), 045006.

Swaminathan, N., Qu, J., Sun, Y., 2007a. An electrochemomechanical theory of defects in ionic solids. I. Theory. Philos. Mag. 87 (11), 1705–1721.

Swaminathan, N., Qu, J., Sun, Y., 2007b. An electrochemomechanical theory of defects in ionic solids. Part II. Examples. Philos. Mag. 87 (11), 1723–1742.

Tikekar, N.M., Armstrong, T.J., Virkar, A.V., 2006. Reduction and reoxidation kinetics of nickel-based SOFC anodes. J. Electrochem. Soc. 153 (4), A654–A663.

Wan, W.H., Zhang, Q.F., Cui, Y., Wang, E.G., 2010. First principles study of lithium insertion in bulk silicon. J. Phys. Condens. Matter 22 (41), 415501.

Yalamac, E., Carry, C., Akkurt, S., 2011. Microstructural development of interface layers between co-sintered alumina and spinel compacts. J. Eur. Ceram. Soc. 31 (9), 1649–1659.

Yang, F.Q., 2010. Effect of local solid reaction on diffusion-induced stress. J. Appl. Phys. 107 (10), 103516.
Yang, H., Huang, S., Huang, X., Fan, F.F., Liang, W.T., Liu, X.H., Chen, L.Q., Huang, J.Y., Li, J., Zhu, T., Zhang, S.L., 2012. Orientation-dependent interfacial mobility governs the anisotropic swelling in lithiated silicon nanowires. Nano Lett. 12 (4), 1953–1958.
Zhang, Q., White, R.E., 2007. Moving boundary model for the discharge of a $LiCoO_2$ electrode. J. Electrochem. Soc. 154 (6), A587–A596.
Zhang, Q.F., Zhang, W.X., Wan, W.H., Cui, Y., Wang, E.G., 2010. Lithium insertion in silicon nanowires: an ab initio study. Nano Lett. 10 (9), 3243–3249.
Zhao, K.J., Pharr, M., Wan, Q., Wang, W.L., Kaxiras, E., Vlassak, J.J., Suo, Z.G., 2012. Concurrent reaction and plasticity during initial lithiation of crystalline silicon in lithium-ion batteries. J. Electrochem. Soc. 159 (3), A238–A243.
Zhao, K.J., Wang, W.L., Gregoire, J., Pharr, M., Suo, Z.G., Vlassak, J.J., Kaxiras, E., 2011. Lithium-assisted plastic deformation of silicon electrodes in lithium-ion batteries: a first-principles theoretical study. Nano Lett. 11 (7), 2962–2967.
Zhou, H.G., Qu, J.M., Cherkaoui, M., 2010. Stress-oxidation interaction in selective oxidation of Cr–Fe alloys. Mech. Mater. 42 (1), 63–71.